processes

MDPI

Article

Analysis of Sedimentation Behavior and Influencing Factors of Solid Particles in CO_2 Fracturing Fluid

Qiang Li [1], Dandan You [1], Qingchao Li [2,*], Fuling Wang [1], Yanling Wang [3,4,*] and Yandong Yang [5]

[1] Faculty of Engineering, China University of Petroleum-Beijing at Karamay, Karamay 834000, China; liqiang202403@cupk.edu.cn (Q.L.); 2024016971@st.cupk.edu.cn (D.Y.); wangfl@cupk.edu.cn (F.W.)
[2] College of Energy Science and Engineering, Henan Polytechnic University, Jiaozuo 454000, China
[3] College of Petroleum Engineering, China University of Petroleum (East China), Qingdao 266580, China
[4] Key Laboratory of Unconventional Oil & Gas Development, China University of Petroleum (East China), Ministry of Education, Qingdao 266580, China
[5] School of Petroleum Engineering and Environmental Engineering, Yan'an University, Yan'an 716000, China; ycz1021909225@163.com
* Correspondence: liqingchao2020@hpu.edu.cn (Q.L.); wangyl@upc.edu.cn (Y.W.)

Abstract

The fast settling rate of solid particles in the CO_2 fracturing fluid is a serious obstacle to ensuring the smooth progress of reservoir stimulation during conventional energy extraction, exerting a critical influence on enhancing both transformation efficiency and crude oil recovery. In this study, a fluid–solid coupling numerical model was developed, incorporating reservoir conditions and fluid properties, to simulate the settling behavior of solid particles in geological reservoir fluids. In addition, the effects of various geological factors and fluid parameters on particle settling were systematically examined. Furthermore, molecular dynamics theory, together with the analysis of intermolecular bonding interactions, was employed to elucidate the underlying mechanisms governing particle settling under different conditions. The findings of this study have the potential conclusion that the numerical model constructed in this study showed a high degree of fit (98.7%) with the experimental data, demonstrating the high applicability and good match of the numerical model. Furthermore, CO_2 viscosity is a significant factor influencing the differential settling of particles in reservoir fluids, and CO_2 fracturing fluid at 8 mPa·s can reduce the settling distance and velocity of solid particles to 3.2 m and 0.21 m/s, respectively. Simultaneously, both high reservoir pressure and a rough surface can effectively suppress the settling behavior of solid particles in CO_2 fracturing fluid, reducing the settling distance to 3.4 cm and 3.8 cm, respectively. However, the utilisation of high-temperature reservoirs at 383 K has been demonstrated to reduce the particle settling distance to 3.5 cm, a phenomenon that is evidently not conducive to the stimulation of deep, high-temperature reservoirs. The findings of this research endeavour have the potential to provide fundamental data for the utilisation of CO_2 fracturing fluids in reservoir stimulation and EOR.

Keywords: reservoir transformation; CO_2 fracturing fluid; petroleum engineering; enhanced oil recovery; particle sedimentation

check for updates

Academic Editor: Shunde Yin

Received: 10 November 2025
Revised: 7 December 2025
Accepted: 11 December 2025
Published: 15 December 2025

Citation: Li, Q.; You, D.; Li, Q.; Wang, F.; Wang, Y.; Yang, Y. Analysis of Sedimentation Behavior and Influencing Factors of Solid Particles in CO_2 Fracturing Fluid. *Processes* **2025**, *13*, 4049. https://doi.org/10.3390/pr13124049

Copyright: © 2025 by the authors. Licensee MDPI, Basel, Switzerland. This article is an open access article distributed under the terms and conditions of the Creative Commons Attribution (CC BY) license (https://creativecommons.org/licenses/by/4.0/).

1. Introduction

The strong correlation between rapid economic development and the extensive use of fossil fuels has exerted a direct and positive influence on human civilization, as evidenced by substantial increases in industrial productivity and significant improvements

in living standards [1,2]. However, the sustained large-scale extraction of fossil fuels has progressively impeded industrial advancement, thereby intensifying the need for more sophisticated strategies to promote energy development and diversification [3,4]. In response, researchers in the fields of energy and materials science have undertaken a series of initiatives to mitigate the increasing depletion of fossil resources, with particular emphasis on the development of novel energy sources and unconventional energy technologies [5,6]. (1) New energy. Wind, solar, and hydrogen energy have emerged as prominent research frontiers in materials science and energy science, serving as important supplements to mitigate the escalating global energy crisis [7,8]. Nevertheless, the relatively low collection efficiency of these energy sources prevents them from fully substituting fossil fuels in the short term. Moreover, their dependence on climatic conditions and weather variability hinders the provision of a stable and continuous energy supply, limiting large-scale application and promotion [9,10]. In addition, the surplus energy generated during periods of high resource availability (e.g., strong solar radiation or high wind speeds) cannot be fully absorbed due to the limited storage capacity of current energy storage technologies, leading to significant energy waste [11,12]. Consequently, the low storage capacity of energy storage systems, coupled with the inherent intermittency of renewable energy sources, restricts their widespread adoption in industrial production [13,14]. (2) Unconventional energy. Unconventional energy resources, including shale oil, methane hydrates, and reservoir hydrogen, are distributed within unique geological formations and have attracted increasing attention as promising energy alternatives [15,16]. These resources can, in principle, be extracted in the short term using technologies similar to those employed for conventional fossil fuels [17,18]. However, the lack of mature reservoir stimulation and modification technologies has significantly constrained large-scale development and industrial deployment. Consequently, the limitations of existing reservoir modification strategies in unconventional formations have emerged as a critical challenge that requires urgent resolution, as they exert a direct influence on energy security and the trajectory of human societal advancement [19,20].

Reservoir stimulation technologies such as flooding, acidizing, and fracturing are widely applied in the extraction of unconventional energy resources, with fracturing emerging as a pivotal technique for enhancing tertiary oil recovery [21,22]. Various fracturing approaches—including water-based, oil-based, N_2 foam, and CO_2 fracturing—have demonstrated effective fracture propagation in unconventional reservoirs [23,24]. Among them, CO_2 fracturing is regarded as the most promising method due to its favorable environmental performance and moderate fracturing capacity [25,26]. In addition, CO_2 fracturing circumvents the water sensitivity issues associated with water-based fracturing fluids in low-permeability reservoirs, thereby providing distinct advantages in terms of geological protection and permeability preservation [27,28]. Nevertheless, CO_2 fracturing technology still encounters substantial limitations that restrict its large-scale application in unconventional energy extraction [29,30]. The inherently low viscosity, high leak-off rate, weak proppant-suspension capacity, and severe fingering of CO_2 fracturing fluids all pose significant challenges [31,32]. Current mitigation strategies primarily rely on the incorporation of CO_2 thickeners (including fluorinated, hydrocarbon-based, and siloxane-based additives); however, their limited thickening efficiency remains a fundamental bottleneck that must be resolved for the broader deployment of CO_2 fracturing [33,34]. Concurrently, researchers are actively investigating the seepage behavior, proppant-carrying capacity, and fingering characteristics of CO_2 fracturing fluids in unconventional reservoirs [35,36]. Nevertheless, advancements in these properties remain constrained by the intrinsically low viscosity of CO_2, which limits substantial breakthroughs. Li et al. have pursued molecular-level modifications and developed specialized testing equipment for siloxane-based thickeners [37,38],

while also examining key properties of CO_2 fracturing fluids—including phase transition behavior, filtration performance, adsorption characteristics, and proppant transport—within the framework of existing thickening capacity [39–41]. However, the suspension and settling behavior of solid particles in CO_2 fracturing fluids has not yet been systematically investigated [42,43]. In parallel, other researchers have primarily relied on numerical models to evaluate the factors influencing particle settling, without proposing targeted strategies for improvement [44,45].

This study built upon current research on the viscosity regulation and sediment-suspending capacity of CO_2 fracturing fluids. It constructed a numerical model and experimental evaluation device to explore the sediment-suspending behaviour of CO_2 fracturing fluids under various factors. Furthermore, molecular dynamics theory was used to elucidate the proppant suspension mechanism of solid particles in CO_2 fracturing fluids. The adsorption behaviour of microscopic molecules during the sedimentation of solid particles was also incorporated into this discussion. This study integrates physical experimentation with numerical modelling to systematically investigate the sedimentation behaviour of solid particles in CO_2 fracturing fluids under multiple influencing factors, thereby providing essential computational support for CO_2 fracturing in unconventional reservoirs.

2. Numerical Model

2.1. Temperature Fields of Fluids and Rock Solids in Geological Reservoirs

2.1.1. Solid–Liquid Heat Transfer Equation Considering Fluid Viscosity

Previous studies have demonstrated that key parameters of CO_2 fracturing fluids, such as viscosity and seepage capacity, are strongly influenced by reservoir temperature [46,47]. This highlights the necessity of analyzing heat transfer processes between CO_2 and reservoir rocks, as these thermal interactions play a decisive role in governing the sedimentation behavior of solid particles in CO_2 fracturing fluids [48,49]. Equation (1) represents the general energy conservation equation governing fluid–rock interactions in geological reservoirs [50,51], and it provides a universally applicable framework for describing heat transfer and energy distribution between the fluid and solid phases in nearly all types of geological reservoirs [52,53].

$$\rho C_p \frac{\partial T}{\partial t} + \rho_f C_p v \cdot \nabla T = \nabla \cdot (k \nabla T) + Q \quad (1)$$

where ρ and ρ_f are considered as the density of reservoir rocks and geological fluids, kg/m^3. C_p presented the specific heat capacity, $kJ/(kg \cdot ^\circ C)$. T displayed the reservoir temperature, $^\circ C$. t presented the time that geological fluids work on reservoir rocks. v is the flow velocity of geological fluids, which can be determined by the Navier–Stokes equations, m/s. k presented the thermal conductivity of reservoir rock, $W/(m \cdot K)$. Q is the geological heat, W/m^3.

However, Equation (1) does not incorporate the effects of CO_2 viscosity on solid–liquid heat transfer, and thus fails to accurately capture the influence of variations in geological fluid parameters on reservoir heat transfer [54,55]. In contrast, Equation (2) introduces CO_2 viscosity into the energy conservation framework, providing a more rigorous description of the coupling between CO_2 viscosity and reservoir heat transfer, which is of significant importance for understanding their interrelationship [56,57].

$$\rho C_p \frac{\partial T}{\partial t} + \rho_f C_p v \cdot \nabla T = \nabla \cdot (k \nabla T) + Q \quad (2)$$

where e presented the rock permeability of geological reservoirs, m^2. x presented the axial distance of fluid along reservoir fractures, m.

2.1.2. Heat Transfer Equation in a Wellbore Considering Seepage and Thermal Convection

Previous studies have examined the influence of CO_2 viscosity on fluid seepage behavior in geological reservoirs. Accordingly, the fluid–solid heat transfer model for such reservoirs should also incorporate the effects of seepage-related factors into the energy conservation equation (Equation (3)) [58,59].

$$\int_{\Omega} \omega(\rho C_p)_{eff} \frac{\partial T}{\partial t} d\Omega + \int_{\Omega} \omega \rho_f C_{pf} v \nabla T d\Omega + \int_{\Omega} \nabla \omega (e \nabla T) d\Omega = \int_{\Omega} \nabla \omega Q d\Omega + \int_{\partial\Omega} \omega q dS \quad (3)$$

where Ω is the spatial area of geological reservoirs, m^3. ω is the finite element basis functions, which are used to discretize the temperature field. q is the heat flux on the reservoir boundary, W/m^2. dS is the differential area on a surface, m^2.

Furthermore, the geothermal temperature of geological reservoirs has been demonstrated to induce substantial thermal convection in CO_2 fluids. This, in turn, has been shown to result in alterations to the temperature field and the temperature control equation (Equation (4)) [60,61].

$$\rho_f C_p \left(\frac{\partial T}{\partial t} + vz \frac{\partial T}{\partial t}\right) = \nabla \cdot (k_f \nabla T_f) + \frac{2h}{r_w}(T_w - T_f) \quad (4)$$

where r_w and Δ_Z are the fracture inner diameter and fracture length, m. h and T_w are the convective heat transfer coefficient and rock surface temperature. k_f and T_f are thermal conductivity of CO_2 in reservoir fractures and real-time temperature of CO_2.

The momentum equation of solid particles in CO_2 fracturing fluid is shown in Equation (5).

$$\frac{\partial}{\partial t}(\alpha_s \rho_s v) + \nabla \cdot (\alpha_s \rho_s v) = -\alpha_s \nabla p + \nabla \tau_s + \alpha_s \rho_s g + M_{fs} + F_{other} \quad (5)$$

where α_s is the solid phase volume fraction. ρ_s is the particle density. p is the fluid phase pressure. τ_s is the particle stress tensor. g is the gravitational acceleration. M_{fs} is the interphase momentum exchange term. F_{other} is the other forces, which can be ignored in settlement behavior.

2.2. Continuity Equation of CO_2 Fracturing Fluid in Geological Reservoirs

As a unique fluid system, CO_2 fracturing fluid must account for a range of abrupt phenomena—such as phase transitions, multiphase flow, and non-Darcy flow—that significantly influence the settling behavior of solid particles during its migration through geological reservoirs. Accordingly, the continuity equation of CO_2 fracturing fluid in geological reservoirs (Equation (6)) should comprehensively incorporate these factors to accurately capture the governing physical processes [62,63].

$$\frac{\partial(\phi \rho_f G_f)}{\partial t} + \nabla(\rho_f v) = q_f \quad (6)$$

where G_f is the Saturation of CO_2 fracturing fluid. q_f is the injection volume of CO_2 fracturing fluid. ϕ is the porosity of geological reservoirs.

The Darcy velocity of CO_2 fracturing fluid flowing in the reservoir in Equation (5) can be solved using Equation (7) [64,65].

$$v = -\frac{e_{rf}}{\mu} \cdot (\nabla P_f - \rho_f g) \quad (7)$$

where e_{rf} is the relative permeability of CO_2 fracturing fluid, which depends primarily on the van Genuchten model (Equation (8)) related to the fluid saturation S. P_f is the fluid pressure of CO_2 fracturing fluid [66,67]. μ is the reservoir fluid viscosity, mPa·s.

$$e_{rf} = \sqrt{1 - S_w}\left[1 - (S_w)^{1/m}\right]^{2m} \quad (8)$$

where S_w is the residual saturation of the wetting phase (water). m is a model parameter, which is usually related to the reservoir pore structure.

2.3. Model Boundary Conditions Between Particles and Fracturing Fluid in Geological Reservoirs

The numerical model was established within a geological reservoir fracture, with the computational domain defined as a cylindrical region of 1 cm in diameter. The fracture was oriented horizontally, and solid proppant particles were allowed to free-fall from the top. The particles were assigned an elastic modulus of 55 GPa, a Poisson's ratio of 0.24, and a stiffness of 2.4×10^7 N/m to accurately account for mechanical deformation under compressive loading during particle closure [68,69].

The pressure boundaries were set at 30 MPa on the left and 14 MPa on the right, establishing a pressure gradient of 3 MPa per 2 cm to drive the lateral flow of CO_2 fracturing fluid along the reservoir fracture. The lateral fracture boundaries were defined as no-flow conditions to simulate a closed system, with fluid motion governed by the cubic law. Additionally, the model assumed constant fluid properties, temperature, and pressure during particle descent, and the longitudinal forces acting on the particles were considered unaffected by the fluid flow [70,71].

The maximum horizontal and vertical stresses in the numerical model were set to 48 MPa and 45 MPa, respectively. The tensile strain and particle porosity were defined as 0.05% and 11%, respectively, to prevent excessive deformation caused by external pressure and particle–fluid interactions.

Finally, the CO_2 fracturing fluid within the reservoir fractures was modeled as a single-phase, slightly compressible fluid, with viscosity ranging from 0.04 to 10 mPa·s.

2.4. Construction of a Multi-Coupled Performance Evaluation Device for CO_2 Fracturing Fluid

The multi-coupled performance evaluation device for CO_2 fracturing fluid is composed of four constituent parts: phase behaviour evaluation, fluid rheology, particle settling behaviour, and core analysis (as shown in Figure S1 in the Supplementary Materials). Initially, pressurised CO_2 fracturing fluid, propelled by a pressurisation pump, is injected into a pressure-resistant container equipped with a viewing window and stirred to homogenise, allowing for the identification of the phase behaviour of the miscible CO_2 fracturing fluid. The highly soluble CO_2 fracturing fluid is then injected into a capillary viscometer for rheological parameter evaluation, which helps determine the applicable viscosity range for a specific reservoir. Concurrently, the CO_2 fracturing fluid is subjected to further pressurisation and pumped into a particle settling apparatus, thereby facilitating the evaluation of particle settling behaviour under varying conditions. Subsequent to the evaluation of the settling behaviour of the CO_2 fracturing fluid, it is injected into a core sample for the purpose of conducting core fracture propagation experiments.

2.5. Model Decoupling, Solution and Adaptability Validation of Investigation Methodology

2.5.1. Model Decoupling, Solution

The equivalent integral form of the continuity equation (energy conservation equation) (Equation (1)) for the CO_2 fracturing fluid and settling particle model in reservoir fractures can be written as Equation (9) [72,73].

$$\frac{\partial}{\partial t}\int_v \rho_f C_p T dv + \oint_{\partial v} \rho_f C_p T(vn) dS = \oint_{\partial v} k\frac{\partial T}{\partial n} dS + \int_v Q dv \tag{9}$$

where n represents the unit normal vector of each point on the boundary surface.

Simultaneously, a weak form analysis of the mass conservation equation (Equation (10)) was conducted to improve the numerical model's stability and mitigate the influence of high-frequency noise.

$$\int_0^H w\frac{\partial \rho_f}{\partial t} dz - \int_0^H (\rho_f v_z)\frac{\partial w}{\partial z} dz + \int_0^H w\left(\frac{2}{r_w}\rho_f v_r\Big|_{r=r_w}\right) dz = 0 \tag{10}$$

In addition, the temperature control equation (Equation (11)) was reformulated into a weak integral form to improve the stability and convergence of the numerical model. [66,67].

$$\begin{aligned} &\int_0^H w\rho_f C_{pf}\frac{\partial T_f}{\partial t} dz + \int_0^H \rho_f C_{pf} v_z \frac{\partial T_f}{\partial z} w dz + \int_0^H k_f \frac{\partial T_f}{\partial z}\frac{\partial w}{\partial z} dz \\ &+ \frac{2h}{r_w}\int_0^H w T_f dz = \frac{2h}{r_w}\int_0^H w T_w dz \end{aligned} \tag{11}$$

where T_w is the well wall temperature. r_w is the wellbore radius. C_{pf} is the specific heat capacity of CO_2 fracturing fluid.

The particle sedimentation model of CO_2 fracturing fluid within reservoir fractures (Figure 1) neglects the influence of fluid seepage on reservoir pressure and rheological parameters. Accordingly, the seepage equation and its corresponding weak integral form are not considered in this investigation.

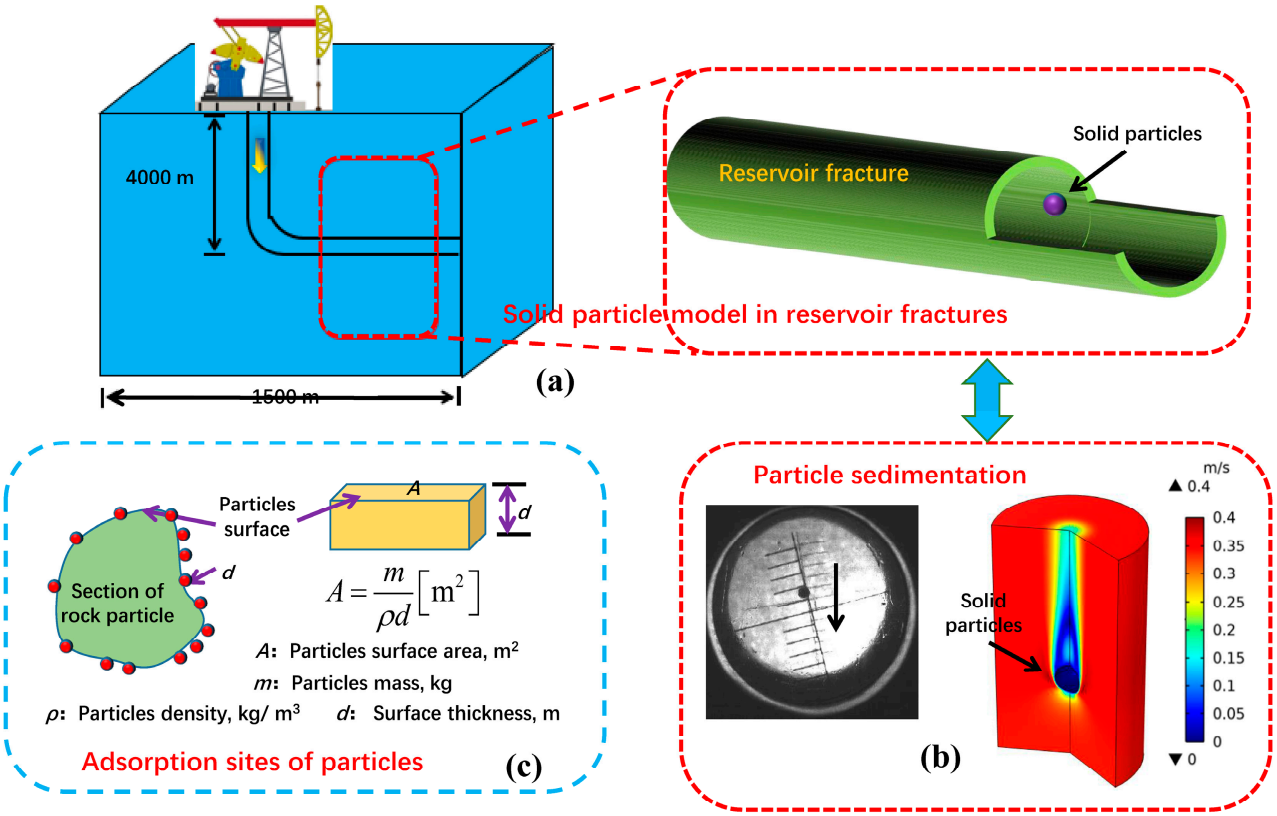


Figure 1. The sedimentation model of solid particles in reservoir fractures in CO_2 fracturing fluid. (**a**): Geometry Model. (**b**): Particle sedimentation model. (**c**): Theory of material adsorption on particle surface.

2.5.2. Adaptability Validation of Investigation Methodology

The comparative analysis between this numerical model and the experimental data from previous studies is shown in Figure 2 [74]. A comparison of the two sets of data indicates that the particle settling trend of the numerical model is similar to the experimental results in terms of variation trend. Concurrently, the compatibility between the two components is noteworthy, exhibiting excellent similarity characteristics (R^2 = 98.7%). This facilitates expeditious and precise data acquisition, thereby substantiating the efficacy of numerical models in simulating particle settling behaviour within reservoir fractures. However, a slight discrepancy has been identified between the two sets of data previously mentioned due to the differences between the simplified, ideal experimental conditions and the complex interfering factors considered in the numerical model. The numerical model incorporates the impact of alterations in fluid flow state on the process of particle settling, while experimental data is regarded as ideal, stemming from static fluid conditions devoid of pressure gradients. The impact of fluid flow and various interfering factors on particle settling has only been analysed through numerical simulations, which requires further exploration and data verification on the later construction of experimental equipment.

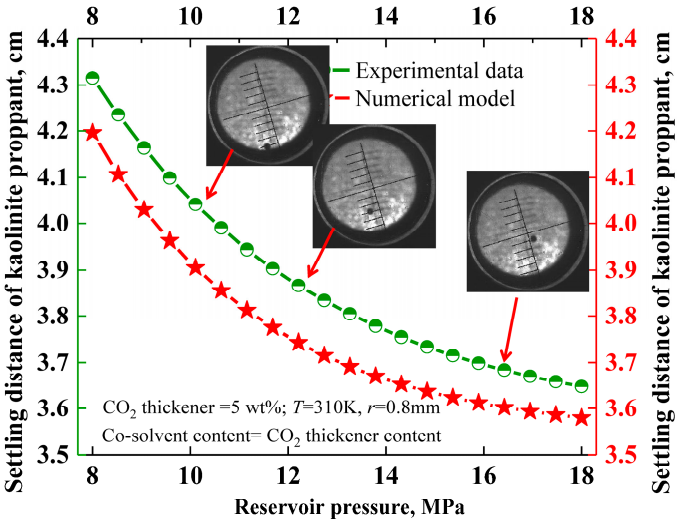


Figure 2. Comparison of confirmatory data between preliminary research and numerical models.

3. Results and Discussion

3.1. The Influence of CO_2 Fluid Viscosity on Particle Settling Behavior

The settling behaviour of solid particles within reservoir fractures filled with CO_2 fracturing fluid is strongly governed by key fluid parameters, among which fluid viscosity serves as a primary determinant of variations in particle settling dynamics. As shown in Figure 3, the influence of reservoir fluid viscosity on particle settling distance provides a valuable reference for selecting appropriate CO_2 fracturing fluid formulations—particularly with respect to viscosity and composition—for different geological reservoirs. An inverse correlation is observed between particle settling distance and the viscosity of the CO_2 fracturing fluid (Figure 3). These results indicate that low-viscosity CO_2 fracturing fluid promotes the rapid settling of particles to the bottom of reservoir fractures. The settling distance of particles decreases with increasing CO_2 fluid viscosity; however, the rate at which this reduction occurs varies across different viscosity ranges. When the CO_2 viscosity is below 5 mPa·s, the decline in settling distance is relatively minor, decreasing by only 0.2 cm—from 5.2 cm at 3 mPa·s to 5.05 cm at 5 mPa·s. Once the viscosity exceeds 5 mPa·s, the reduction rate accelerates substantially, with the settling distance decreasing by 1.8 cm as the viscosity increases from 5 to 8 mPa·s.

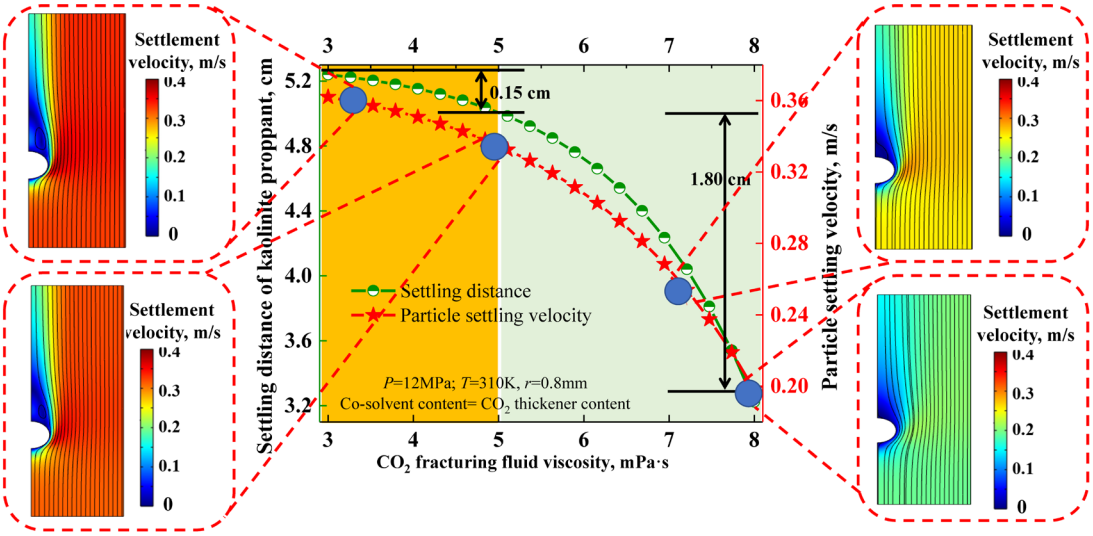


Figure 3. Particle settling velocity and settling distance corresponding to different fluid viscosities.

The proportional relationship between particle settling behaviour and the viscosity of CO_2 fracturing fluid can be elucidated by examining intermolecular forces and adsorption mechanisms, which inherently involve the three-dimensional mesh theory of CO_2 fracturing fluids [75,76]. Previous studies have demonstrated that CO_2 viscosity is primarily governed by intermolecular chemical bonding and van der Waals interactions among CO_2 molecules, cosolvents, and thickeners, which collectively generate a three-dimensional mesh structure. The density of this mesh directly dictates the viscosity-enhancement trend of CO_2 fracturing fluid [77,78]. It is generally recognised that a denser micro-mesh corresponds to higher CO_2 viscosity, whereas lower viscosity is associated with a more loosely connected mesh network [79,80]. At the microscopic scale, lower fluid viscosity arises from the presence of only a limited number of intermolecular bonds, which are insufficiently strong to hinder the vertical settling of particles. The expression for particle–fluid settling resistance in CO_2 fracturing fluid, provided in Equations (12) and (13) [81,82], likewise demonstrates a direct proportional relationship between settling resistance and fluid viscosity. This relationship primarily results from the reduced number of chemical bonds within low-viscosity fluids. In highly viscous fluids, the intermolecular bonds form a relatively stable and slowly deforming mesh structure that effectively impedes the rapid downward motion of solid particles. By contrast, in low-viscosity fluids, the sparse and weak intermolecular bonding network cannot respond rapidly enough to generate meaningful resistance, thereby allowing particles to settle more freely.

$$C_D = \frac{24}{\mathrm{Re}}(1 + 0.1118(\phi^{0.4305}\mathrm{Re})^{0.6567}) + \frac{0.4305\phi^{-1.88}}{1 + 3305/(\phi^{0.4305}\mathrm{Re})} \tag{12}$$

$$\mathrm{Re} = \frac{\rho_f u D}{\mu} \tag{13}$$

where C_D is the drag coefficient of solid particles. *Re* is the Reynolds number under flowing conditions. ϕ is the particle roundness. *D* is the Inner diameter of reservoir fracture. *u* is the average flow velocity of the pipe cross-section.

The microgrid formed by intermolecular chemical bonds in CO_2 fracturing fluid can be regarded as two-fold [83]: firstly, as a barrier to particle settling, and secondly, as an effective means of resisting the adsorption behaviour of chemical substances on the surface of particles in CO_2 fracturing fluid. Furthermore, the disparity in fluid viscosity of the CO_2 fracturing fluid can also engender discrepancies in adsorption and settling abilities, which

can significantly impact resistance during particle settling (Figure 4). The adsorption of substances on particle surfaces is primarily driven by the interaction between the polar groups present on the particle surface (the outermost hydroxyl group in kaolinite) and the polar groups (ether groups) of thickeners in fracturing fluids [84,85]. This interaction results in the formation of a tight and similar "rivet effect" between the two, thereby promoting the adsorption of substances on solid particle surfaces [86,87]. Concurrently, chemical substances exhibit a high degree of immobility within the CO_2 fracturing fluid due to the microgrid constructed by other substances, thereby engendering relatively static chemical bonds that impede the mobility of falling solid particles through the target points on the particle surface (the outermost OH in kaolinite) [88,89]. The higher apparent viscosity of CO_2 fracturing fluid is indicative of a greater chemical composition, which in turn leads to an increased "rivet effect" and drag force at high viscosity. The aforementioned description naturally gives rise to two vertical upward forces, which collectively generate the resistance that prevents the descent of solid particles. It is evident that high viscosity can effectively augment the aforementioned two forces that constitute the vertical upward resistance [90,91]. However, the employment of a low viscosity CO_2 fracturing fluid does not merely construct a sparse micro grid, thereby weakening the effective barrier to large solid particles; it also serves to reduce the particle descent resistance due to insufficient adsorption of polar groups in the CO_2 fluid on the surface of solid particles [92,93]. Consequently, low viscosity CO_2 fracturing fluids manifest larger particle settling distances macroscopically, while high viscosity fluids can effectively mitigate particle settling behaviour.

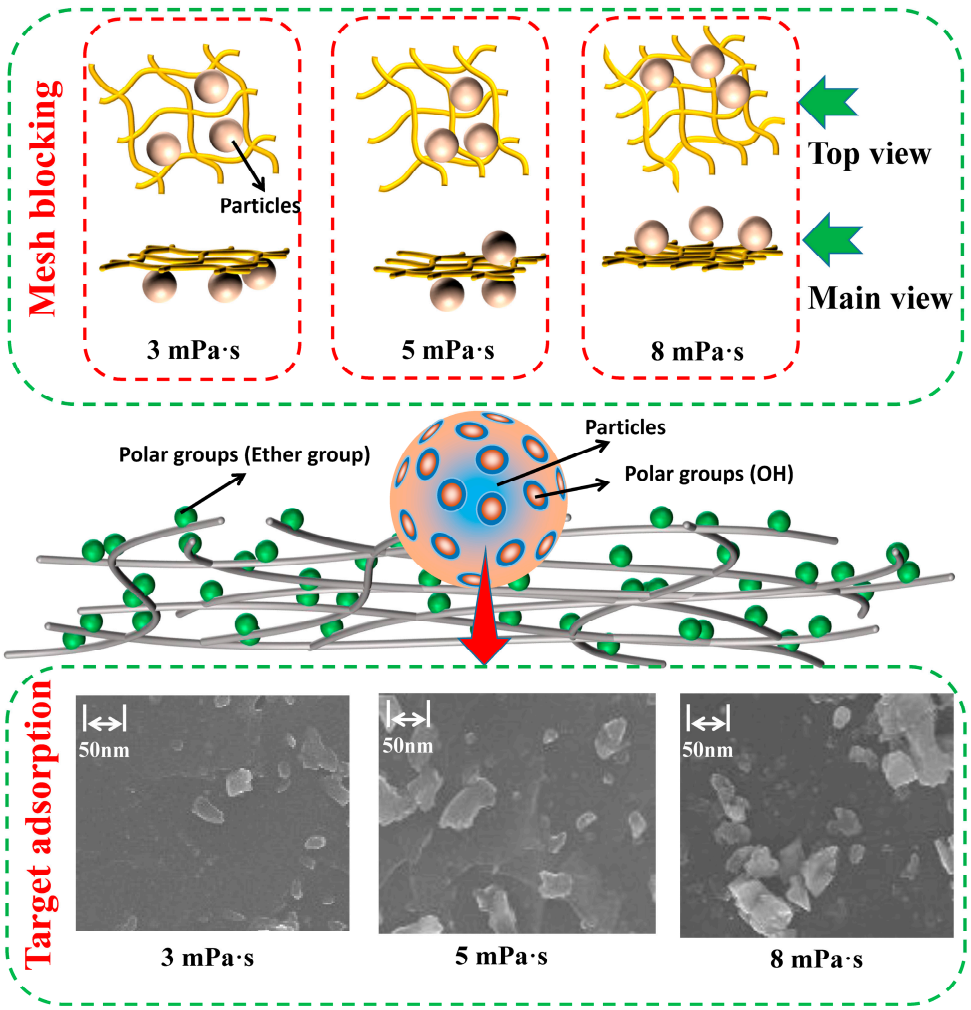


Figure 4. Mechanism analysis of particle sedimentation under different viscosities.

3.2. Influence and Mechanism Analysis of Particle Roughness on Settlement Behavior

The above analysis indicates that the sedimentation behavior of solid particles in CO_2 fracturing fluid within reservoir fractures is primarily governed by two mechanisms: microscopic mesh blockage and particle surface adsorption. Microscopic mesh blockage arises mainly from differences in particle size, with minimal dependence on surface roughness [94,95]. In contrast, particle surface adsorption is dominated by "rivet-like adsorption" between polar groups on the particle surface and those within the CO_2 fracturing fluid, which is directly influenced by particle surface roughness. Therefore, investigating the effect of surface roughness on particle sedimentation in CO_2 fracturing fluid is of significant importance, as it aids in selecting optimal solid particles for specific reservoir conditions. Figure 5 presents the characteristic curves of particle sedimentation and the corresponding variations in surface adsorption under different roughness levels, illustrating the causal relationship between sedimentation behavior and adsorption intensity.

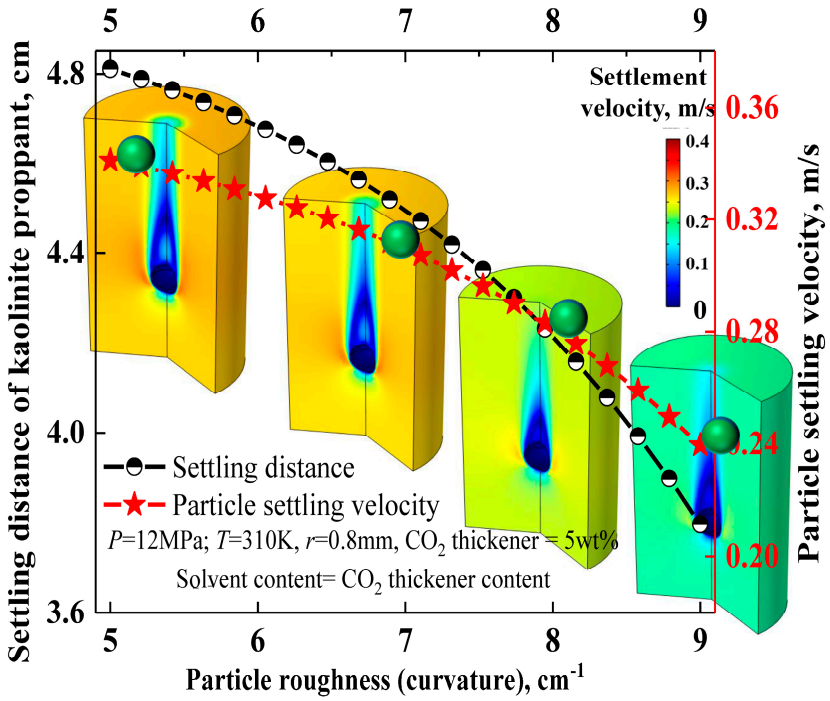


Figure 5. Variation in settling distance and settling velocity under different particle roughness.

As demonstrated in Figure 5, a discernible inverse correlation is evident between the settling distance of particles and their respective roughness. In contrast, a robust positive correlation is observed between the settling velocity of particles and the distance over which they settle. It is generally accepted that an increase in particle roughness is detrimental to the process of particle settling. However, a decrease in particle roughness has been shown to have no significant impact on the aforementioned process. Conversely, an increase in particle roughness has been shown to result in a substantial decrease in suspension or settling velocity, a phenomenon that is advantageous for the effective support of geological reservoir fractures and reservoir stimulation. In this paper, the term "curvature" is employed in lieu of "roughness" to investigate the impact of particle roughness on particle settling behaviour, thereby facilitating the quantification of the relationship between the two parameters. As demonstrated in Figure 5, the curvature of less than 7 cm^{-1} has minimal impact on the settling behaviour of solid particles in CO_2 fracturing fluid; the settling distance exhibits a decline from 4.8 cm at 5 cm^{-1} to 4.5 cm at 7 cm^{-1}. However, particle curvature greater than 7 cm^{-1} exhibits rapid solid settling behaviour, with the settling distance decreasing rapidly from 4.5 cm at 7 cm^{-1} to 3.8 cm at 9 cm^{-1}.

The inverse relationship between particle settling and particle roughness is primarily attributed to two factors: shape resistance and adsorption resistance (Figure 6). Firstly, it is evident that regular spherical particles with smaller curvature exhibit less shape resistance during settling, which inevitably facilitates rapid settling. Irregular particles with larger curvature experience significant frictional resistance from the relatively stationary CO_2 fluid during descent, thus hindering their rapid settling [96,97]. Furthermore, the effective functional groups in the CO_2 fracturing fluid have been shown to interact effectively with the surface functional groups (target sites) of solid particles, aiding in dragging the descending solid particles. However, under constant fluid composition, the shape of the solid particles directly determines the number of target sites on the particle surface in the CO_2 fracturing fluid. In the context of solid particle surfaces characterised by reduced curvature, i.e., roughness, it is not feasible to guarantee the exposure of a sufficient number of the outermost hydroxyl (OH) layers of the alumina octahedrons on the particle surface. This suggests that the abundant polar functional groups present in the CO_2 fracturing fluid are capable of interacting with only a limited number of functional groups on the particle surface, thereby facilitating the movement of descending particles. The particle target effect, which is relatively weak, and the drag force, which is small, are both insufficient to effectively halt the continuously descending solid particles. It has been determined that particle shape drag plays a significant role in hindering particle settling. Concurrently, although the drag caused by changes in the roughness and curvature of solid particles is an important force in hindering the settling of particles with low curvature, the relatively small shape drag value is still insufficient to effectively alleviate the rapid descent of particles [98,99]. However, greater roughness and shape curvature expose more surface targets due to the increased specific surface area, which facilitates the interaction between the abundant polar groups in the CO_2 fracturing fluid and the rich groups on the particle surface. Stronger interactions can generate a large amount of adsorption, which helps the relatively stationary CO_2 fracturing fluid (vertical direction) effectively drag more rapidly descending solid particles. Simultaneously, the shape change caused by larger roughness of solid particles can also create greater shape drag, which inevitably increases the total resistance during particle settling and achieves rapid blocking of solid particles. Therefore, appropriately increasing the size of solid particles during reservoir stimulation can alter their settling behavior, which helps CO_2 fracturing fluid carry solid particles into deeper reservoirs to support the microfractures after fracturing.

3.3. Effect of Lateral Fluid Flow on the Settling of Solid Particles

Previous studies have primarily employed static fluids as the medium for particle transport, while the influence of lateral CO_2 fracturing fluid flow within reservoir fractures on the settling behavior of solid particles has received limited attention. Figure 7 illustrates the effects of different lateral flow velocities of CO_2 fracturing fluid on the settling distance and velocity of solid particles, which, to some extent more accurately represent actual particle settling behavior in geological reservoirs. As shown in Figure 7, higher lateral flow velocities result in longer particle settling distances, whereas lower flow velocities effectively suppress particle settling. Although a clear positive correlation exists between fluid velocity and particle settling distance, the settling trend varies significantly across velocity ranges. When the fluid velocity is below 10 m/s, the settling distance increases slowly—from 4.6 cm at 7 m/s to 4.9 cm at 10 m/s. However, when the velocity exceeds 10 m/s, the settling distance increases more markedly by approximately 0.8 cm. A similar trend is observed in particle settling velocity, indicating that higher lateral flow velocities exacerbate rather than mitigate particle settling behavior.

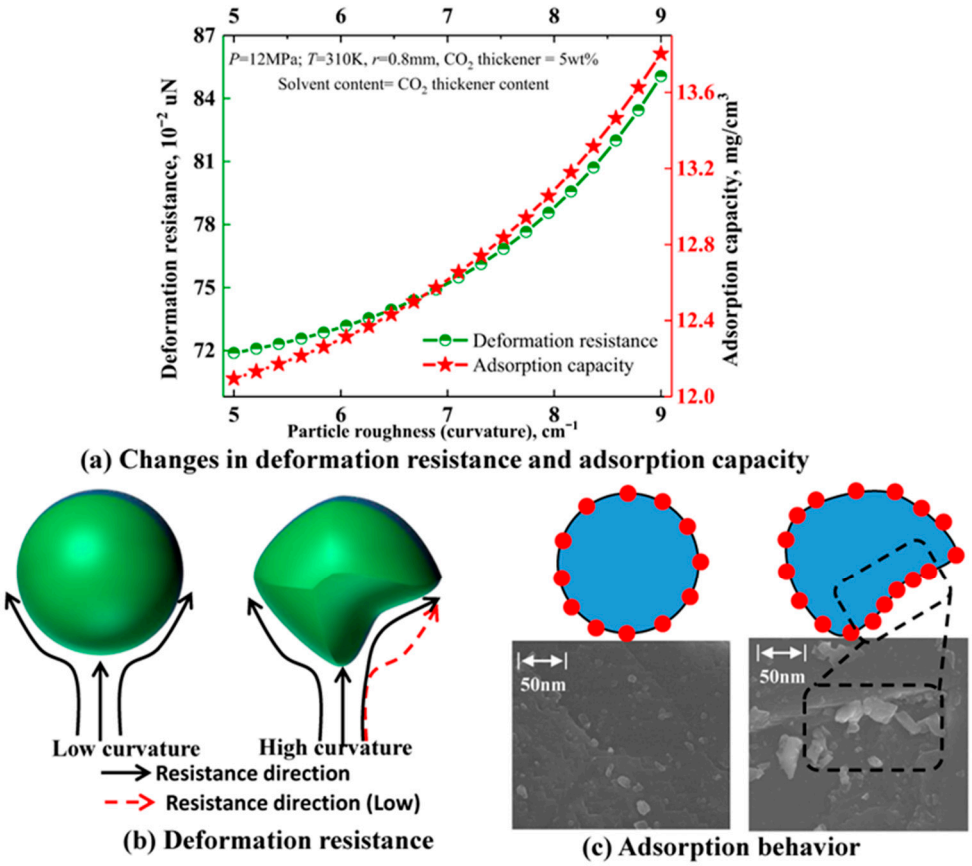


Figure 6. Changes in deformation resistance and adsorption resistance caused by particle curvature (roughness).

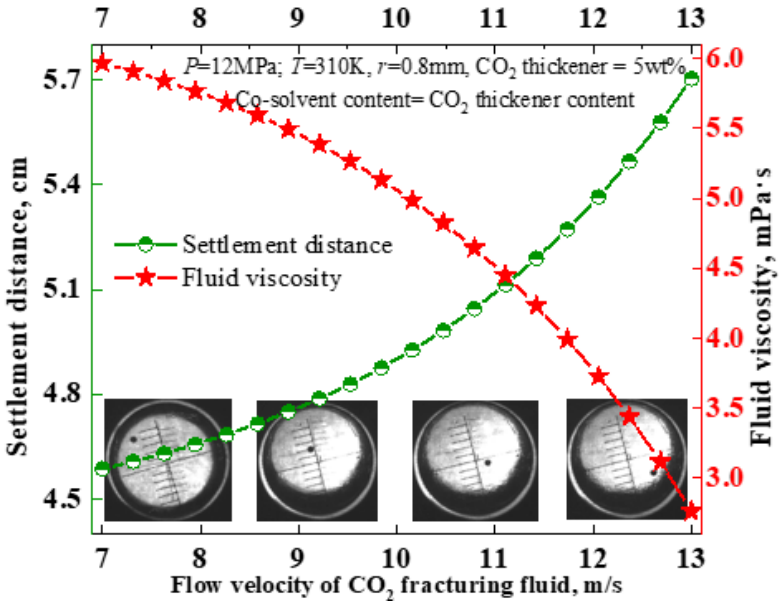


Figure 7. Effects of flow velocity on particle settling and fluid viscosity.

The inverse relationship between particle settling distance and flow velocity is primarily attributed to the shear-induced rupture of intermolecular chemical bonds caused by fluid motion. This process inevitably reduces the microscopic network density and, consequently, decreases the fluid viscosity [100,101]. At low flow velocities, the generated shear stress and shear rate are relatively weak, insufficient to effectively disrupt the

established intermolecular chemical bonds. As a result, only bonds with lower binding energies are partially broken, leading to a minor reduction in the micro-network density of the CO_2 fracturing fluid. This limited decrease in network density only slightly reduces the obstruction posed by the micro-network to solid particles and is insufficient to allow large-scale particle penetration and rapid sedimentation. Simultaneously, the minimal bond breakage at low flow velocities weakens only a small fraction of the surface adsorption forces acting on solid particles, thereby slightly diminishing the drag effect within the micro-network. Consequently, these two mechanisms jointly result in a slight reduction in resistance and drag force at low flow velocities, leading to a gradual increase in the settling distance of solid particles. However, high flow velocities of CO_2 fracturing fluid within reservoir fractures induce extensive breaking and stretching of chemical bonds, thereby disrupting the counteracting forces that hinder particle sedimentation. As the flow velocity increases, the accelerated rupture of intermolecular bonds significantly decreases the micro-network density, which macroscopically fails to obstruct the settling of solid particles. Simultaneously, the bond breakage at high flow rates promotes the desorption of substances originally adsorbed on the particle surfaces, markedly weakening the drag resistance generated by the "rivet effect" [101,102]. Hence, CO_2 fracturing fluids at higher flow velocities rapidly reduce the combined resistance opposing particle settling, primarily due to the decreased network density and weakened adsorption arising from extensive bond shearing and stretching under high shear conditions. In summary, moderately reducing the fluid flow velocity can effectively suppress particle sedimentation; however, the optimal flow rate should be determined by integrating reservoir geological parameters and corresponding fracturing pressures.

3.4. Effect of Reservoir Temperature and Pressure on the Settling Behavior of Solid Particles

Reservoir temperature, as a critical geological parameter, exerts a pronounced influence on the physicochemical properties of CO_2 fracturing fluid and, consequently, represents an important factor governing particle settling behavior. Figure 8 illustrates the relationship between the settling distance and adsorption capacity of solid particles in CO_2 fracturing fluid under varying reservoir temperatures. The two parameters display distinctly opposite trends with increasing temperature: as the reservoir temperature rises, the settling distance of solid particles increases markedly, whereas the adsorption capacity decreases. This inverse relationship indicates a strong causal linkage between adsorption capacity and settling behavior, providing valuable insight into the mechanisms by which temperature variations affect particle sedimentation. As shown in Figure 8, although an increase in reservoir temperature generally enhances particle settling distance, the effect remains relatively limited at lower temperatures. Specifically, the settling distance of solid particles in reservoir fractures increases modestly from 3.6 cm at 333 K to 3.9 cm at 353 K, but rises sharply to 5.4 cm at 383 K.

The variation in particle settling distance with reservoir temperature remains closely associated with the micro-network density and surface adsorption characteristics of the CO_2 fracturing fluid. Reservoir temperature directly affects both the sparsity of the micro-network structure and the drag force arising from adsorption. The influence of temperature on particle settling and network density can be interpreted through the Arrhenius relationship [103], which links molecular activity to activation energy and thus helps elucidate settling behavior via molecular dynamics. At lower reservoir temperatures, the activation energy and molecular kinetic activity of CO_2 fracturing fluid are insufficient to induce significant Brownian motion, limiting the stretching or disruption of intermolecular bonds and micro-network structures. Consequently, the micro-network density remains nearly constant, and its obstruction to particle motion is largely unchanged, resulting in only a

minor increase in settling distance. Meanwhile, reduced molecular activity at low temperatures hinders the desorption of fluid molecules adsorbed onto particle surfaces, thereby maintaining a strong drag force from surface adsorption. Hence, the combined effects of stable micro-network density and persistent surface adsorption at low reservoir temperatures fundamentally account for the slow increase in particle settling distance observed in Figure 8.

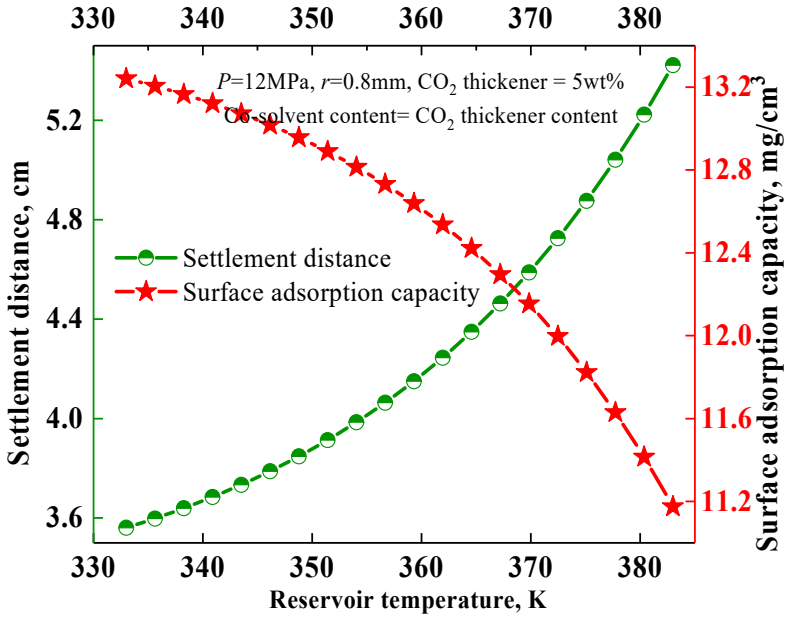


Figure 8. The influence of reservoir temperature on particle settling and surface adsorption in reservoir fractures.

However, increasing reservoir temperature enhances the molecular activity of the CO_2 fracturing fluid, intensifying the irregular Brownian motion of molecules [103,104]. The chemical bonds originally formed between molecules are continuously stretched under thermal agitation, leading to reduced bond stability and elongation of bond lengths due to intermolecular repulsion and motion. These effects collectively decrease the micro-network density of the chemical bond framework [105,106]. Moreover, chemical bonds with relatively low bond energies are more susceptible to shear-induced breakage at elevated temperatures, further diminishing the micro-network density. Consequently, the combined effects of bond stretching and breakage under high temperatures significantly thin the micro-network structure, reducing its ability to hinder solid particle movement and lowering grid-induced resistance [107,108]. Additionally, elevated reservoir temperature affects the adsorption capacity of chemical species on particle surfaces, as molecular activity increases with temperature. The enhanced molecular motion facilitates the desorption of adsorbed species from particle surfaces. Simultaneously, repulsive interactions between electrons in polar groups on both the particle surface and the adsorbed molecules further promote desorption [109,110]. Therefore, although high reservoir temperature is unfavorable for suppressing the settling of solid particles within reservoir fractures, it helps to mitigate excessive adsorption and thereby reduces the potential for reservoir damage.

The influence of reservoir pressure on particle settling behavior exhibits an opposite trend to that of reservoir temperature, facilitating deeper particle migration and improved fracture support in high-pressure reservoirs. Increasing reservoir pressure reduces the particle settling distance while enhancing surface adsorption capacity [111,112]. At relatively low pressures, these changes remain minor; however, when reservoir pressure exceeds 16 MPa, the settling distance decreases markedly, and adsorption capacity increases signifi-

cantly [113,114]. Notably, variations in reservoir pressure at different stages lead to distinct responses in both settling distance and adsorption behavior. As shown in Figure 9 and Table 1, modest pressure increases do not cause substantial reductions in settling distance or notable enhancements in adsorption. In contrast, higher reservoir pressures effectively suppress particle sedimentation and markedly promote the adsorption of chemical species onto particle surfaces. It is evident that under varying reservoir pressures, there is a substantial increase in particle adsorption. However, within the pressure range of 20 MPa, it is not feasible to ascertain monolayer or multilayer adsorption. As demonstrated in Figure 9, the adsorption curve displays a swift rise in adsorption capacity; however, the SEM results indicate incomplete adsorption.

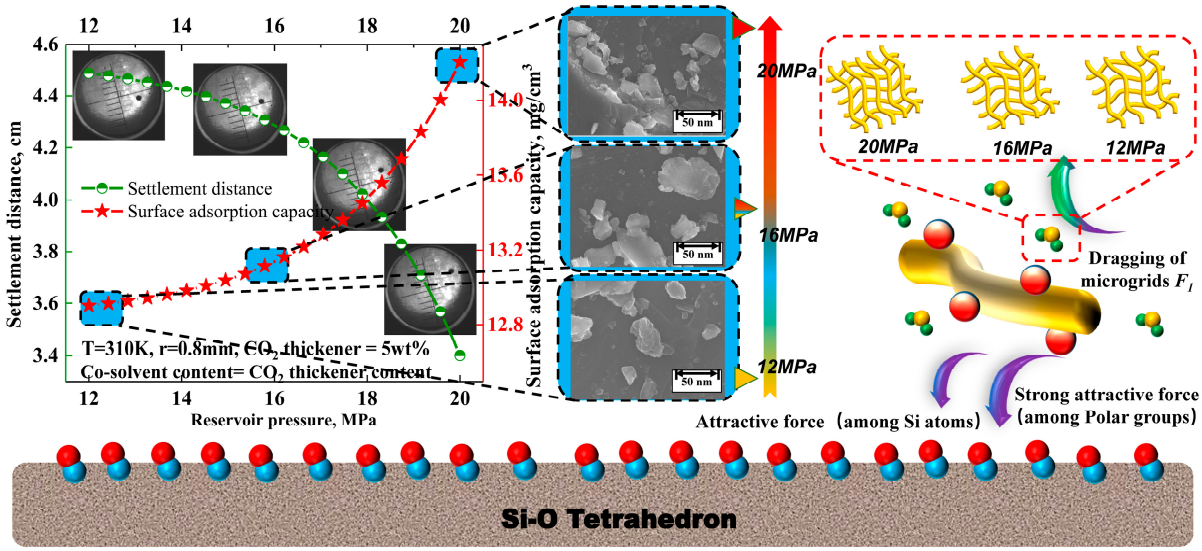


Figure 9. Influence of reservoir pressure on particle settling distance and adsorption behavior.

Table 1. Parameter changes in microgrid and chemical bonds in CO_2 fracturing fluid under different pressures.

Reservoir pressure/MPa	12	14	16	18
Chemical bond length/um	67	65	61	53
Chemical bond energy/$\times 10^{-6}$ J·mol	1.6	1.75	2.08	2.64
Grid density/$\times 10^{3}$ root·um^{3}	2.43	2.51	2.64	2.96

The opposite effects of reservoir pressure and temperature on particle settling primarily originate from changes in chemical bonding, with adsorption capacity serving as a key influencing factor. At low reservoir pressures, the relatively large intermolecular spacing weakens the interactions among CO_2 fracturing fluid molecules, hindering the formation of dense chemical bonds. Consequently, only low-density micro-networks are formed, and even moderate pressure increases fail to markedly enhance their density. Such sparse micro-networks cannot effectively impede the rapid descent of solid particles, resulting in longer settling distances. Moreover, low pressure does not facilitate the migration of chemical species toward particle surfaces, thereby reducing adsorption-induced drag. In contrast, high reservoir pressure significantly compresses intermolecular spacing, promoting both the compaction of existing chemical bonds and the formation of new ones. This compression substantially increases the micro-network density. Simultaneously, high pressure enhances the re-adsorption of chemical species onto particle surfaces, strengthening the "rivet effect" and increasing drag forces [115]. Thus, the densified micro-network effectively restricts

particle motion, while elevated adsorption capacity under high pressure further retards particle settling.

In summary, the settling behavior of particles within reservoir fractures is governed by multiple factors, among which surface adsorption of chemical species in CO_2 fracturing fluids plays a dominant role. Moreover, this study did not account for the influence of fluid seepage on particle settling, which represents an important direction for future investigation. Accordingly, future research will focus on the adsorption behavior of chemical species in unconventional geological reservoirs, with the aim of elucidating the underlying adsorption mechanisms and their comprehensive effects on reservoir stimulation.

4. Conclusions

This study established a numerical model to investigate particle settling behavior in CO_2 fracturing fluid within reservoir fractures, enabling quantitative analysis of the key factors influencing particle migration. The accuracy of the model was validated through a multi-coupled experimental device designed for CO_2 fracturing fluid particle settling. Results indicate that increasing the viscosity of the CO_2 fracturing fluid enhances particle settling velocity, confirming that the three-dimensional micro-network density of the fluid is a primary factor impeding particle motion. Moreover, the adsorption of chemical species from the CO_2 fracturing fluid onto particle surfaces generates significant drag forces, which, together with the micro-network obstruction, counteract the gravitational acceleration of particles. Consequently, identifying chemical components or reservoir parameters that both enhance CO_2 fracturing fluid viscosity and promote surface adsorption represents an effective strategy to regulate particle settling. However, this must be balanced against the potential reservoir damage associated with excessive adsorption. Future work will therefore focus on the dual effects of adsorption on reservoir integrity and CO_2 flow dynamics, providing a theoretical foundation for the efficient development of unconventional low-permeability reservoirs through CO_2 fracturing.

Supplementary Materials: The following supporting information can be downloaded at: https://www.mdpi.com/article/10.3390/pr13124049/s1, Figure S1: The multi-coupling evaluation device of CO_2 fracturing fluid.

Author Contributions: Conceptualization, Q.L. (Qiang Li), Q.L. (Qingchao Li) and D.Y.; methodology, Q.L. (Qingchao Li) and F.W.; validation, Y.W. and Y.Y.; formal analysis, Q.L. (Qiang Li) and Q.L. (Qingchao Li). All authors have read and agreed to the published version of the manuscript.

Funding: This research was sponsored by "Tianchi Talents" Young Doctor Introduction Program Project (2024592109, 2023592120), Henan Provincial Science and Technology Research Project (242102320342), the Fundamental Research Funds for the Universities of Henan Province (NSFRF240616).

Informed Consent Statement: Informed consent was obtained from all subjects involved in the study.

Data Availability Statement: The original contributions presented in this study are included in the article. Further inquiries can be directed to the corresponding author.

Conflicts of Interest: The authors declare no conflicts of interest.

References

1. Wanniarachchi, W.A.M.; Ranjith, P.G.; Perera, M.S.A. Shale gas fracturing using foam-based fracturing fluid: A review. *Environ. Earth Sci.* **2017**, *76*, 1–15. [CrossRef]
2. Satea, A.; Tian, Y.; Kou, Z.; Kang, B.; Zhao, Y.; Zhang, L. A technical review of chemical reactions during CCUS-EOR in different reservoirs. *Nat. Gas Ind. B* **2025**, *12*, 264–278. [CrossRef]
3. Wang, J.; Elsworth, D.; Wu, Y.; Liu, J.; Zhu, W.; Liu, Y. The influence of fracturing fluids on fracturing processes: A comparison between water, oil and SC-CO_2. *Rock Mech. Rock Eng.* **2018**, *51*, 299–313. [CrossRef]

4. Kanninen, M.F. Applications of dynamic fracture mechanics for the prediction of crack arrest in engineering structures. *Int. J. Fract.* **1985**, *27*, 299–312. [CrossRef]
5. Li, Q.; Li, Y.; Cheng, Y.; Li, Q.; Wang, F.; Wei, J.; Ansari, U. Numerical simulation of fracture reorientation during hydraulic fracturing in perforated horizontal well in shale reservoirs. *Energy Sources Part A Recovery Util. Environ. Eff.* **2018**, *40*, 1807–1813. [CrossRef]
6. Papavasileiou, K.D.; Michalis, V.K.; Peristeras, L.D.; Vasileiadis, M.; Striolo, A.; Economou, I.G. Molecular dynamics simulation of water-based fracturing fluids in kaolinite slit pores. *J. Phys. Chem. C* **2018**, *122*, 17170–17183. [CrossRef]
7. Yang, Y.; Niu, J.; Zhang, C.; Liao, H. Simulation analysis of an impeller percussive drilling tool based on rotation law. *Arab. J. Geosci.* **2021**, *14*, 1940. [CrossRef]
8. Hou, L.; Zhang, S.; Elsworth, D.; Liu, H.; Sun, B.; Geng, X. Review of fundamental studies of CO_2 fracturing: Fracture propagation, propping and permeating. *J. Pet. Sci. Eng.* **2021**, *205*, 108823. [CrossRef]
9. Zhang, X.; Zhu, W.; Xu, Z.; Liu, S.; Wei, C. A review of experimental apparatus for supercritical CO_2 fracturing of shale. *J. Pet. Sci. Eng.* **2022**, *208*, 109515. [CrossRef]
10. Zhao, H.; Wu, K.; Huang, Z.; Xu, Z.; Shi, H.; Wang, H. Numerical model of CO_2 fracturing in naturally fractured reservoirs. *Eng. Fract. Mech.* **2021**, *244*, 107548. [CrossRef]
11. Yang, B.; Wang, H.Z.; Li, G.S.; Wang, B.; Chang, L.; Tian, G.H.; Zhao, C.M.; Zheng, Y. Fundamental study and utilization on supercritical CO_2 fracturing developing unconventional resources: Current status, challenge and future perspectives. *Pet. Sci.* **2022**, *19*, 2757–2780. [CrossRef]
12. Li, Q.; Li, Q.; Wang, F.; Wu, J.; Wang, Y.; Jin, J. Effects of Geological and Fluid Characteristics on the Injection Filtration of Hydraulic Fracturing Fluid in the Wellbores of Shale Reservoirs: Numerical Analysis and Mechanism Determination. *Processes* **2025**, *13*, 1747. [CrossRef]
13. Li, Q.; Wu, J.; Li, Q.; Wang, F.; Cheng, Y. Sediment Instability Caused by Gas Production from Hydrate-Bearing Sediment in Northern South China Sea by Horizontal Wellbore: Sensitivity Analysis. *Nat. Resour. Res.* **2025**, *34*, 1667–1699. [CrossRef]
14. Li, H.; Shi, Y. Study on the performance degradation of sandstone under acidification. *ACS Omega* **2020**, *5*, 28333–28340. [CrossRef]
15. Li, Q.; Li, Q.; Wang, F.; Wu, J.; Wang, Y. The carrying behavior of water-based fracturing fluid in shale reservoir fractures and molecular dynamics of sand-carrying mechanism. *Processes* **2024**, *12*, 2051. [CrossRef]
16. Kreipl, M.P.; Kreipl, A.T. Hydraulic fracturing fluids and their environmental impact: Then, today, and tomorrow. *Environ. Earth Sci.* **2017**, *76*, 160. [CrossRef]
17. Yang, Y.; Liao, H.; Xu, Y.; Niu, J.; Yang, L. Theoretical investigation of the energy transfer efficiency under percussive drilling loads. *Arab. J. Geosci.* **2019**, *12*, 175. [CrossRef]
18. Abdelaal, A.; Aljawad, M.S.; Alyousef, Z.; Almajid, M.M. A review of foam-based fracturing fluids applications: From lab studies to field implementations. *J. Nat. Gas Sci. Eng.* **2021**, *95*, 104236. [CrossRef]
19. Li, Q. Reservoir Science: A Multi-Coupling Communication Platform to Promote Energy Transformation, Climate Change and Environmental Protection. *Reserv. Sci.* **2025**, *1*, 1–2. [CrossRef]
20. Wu, G.; Pan, J.; Anwaier, M.; Wu, J.; Xiao, P.; Zheng, L.; Zhu, D. Effect of nano-SiO_2 on the flowback-flooding integrated performance of water-based fracturing fluids. *J. Mol. Liq.* **2023**, *379*, 121686. [CrossRef]
21. Bongole, K.; Sun, Z.; Yao, J.; Mehmood, A.; Yueying, W.; Mboje, J.; Xin, Y. Multifracture response to supercritical CO_2-EGS and water-EGS based on thermo-hydro-mechanical coupling method. *Int. J. Energy Res.* **2019**, *43*, 7173–7196.
22. Liu, L.; Li, Y.; Cao, W.; Wang, T.; Zhang, L.; Feng, X. Coupled thermo-hydro-mechanical-damage modeling of cold-water injection in deep geothermal reservoirs. *J. Rock Mech. Geotech. Eng.* **2025**. [CrossRef]
23. Pouya, A.; Yazdi, P.B. A damage-plasticity model for cohesive fractures. *Int. J. Rock Mech. Min. Sci.* **2015**, *73*, 194–202. [CrossRef]
24. Sinclair, A.R. Heat Transfer effects in deep well fracturing. *J. Pet. Technol.* **1971**, *23*, 1484–1492. [CrossRef]
25. Zhang, C.P.; Ranjith, P.G.; Perera, M.S.A.; Li, X.; Zhao, J. Simulation of flow behaviour through fractured unconventional gas reservoirs considering the formation damage caused by water-based fracturing fluids. *J. Nat. Gas Sci. Eng.* **2018**, *57*, 100–121. [CrossRef]
26. Fan, S.; Zhang, D.; Wen, H.; Cheng, X.; Liu, X.; Yu, Z.; Hu, B. Enhancing coalbed methane recovery with liquid CO_2 fracturing in underground coal mine: From experiment to field application. *Fuel* **2021**, *290*, 119793. [CrossRef]
27. Ahmadpour, V.; Ahmadi, N.; Rezazadeh, S.; Sadeghiazad, M. Numerical analysis of thermal performance in a finned cylinder for latent heat thermal system (LHTS) applications. *Int. J. Heat Technol.* **2013**, *31*, 155–162.
28. Li, Q.; Wang, Y.; Wang, F.; Wu, J.; Usman Tahir, M.; Li, Q.; Liu, Z. Effect of thickener and reservoir parameters on the filtration property of CO_2 fracturing fluid. *Energy Sources Part A Recovery Util. Environ. Eff.* **2020**, *42*, 1705–1715. [CrossRef]
29. Li, Q.; Wang, Y.; Li, Q.; Foster, G.; Lei, C. Study on the optimization of silicone copolymer synthesis and the evaluation of its thickening performance. *RSC Adv.* **2018**, *8*, 8770–8778. [CrossRef]
30. Liao, S.; Zhang, Z.; Hu, J.; Zhang, Y. The influence of stress and natural fracture on a stimulated deep shale reservoir using the boundary element method. *Nat. Gas Ind. B* **2025**, *12*, 298–315. [CrossRef]

31. Yang, Y.; Huang, F.; Yan, D.; Liao, H.; Niu, J. Characteristic analysis of a HDR percussive drilling tool with sinusoidal impact load. *Geoenergy Sci. Eng.* **2024**, *238*, 212847. [CrossRef]
32. Wang, F.; Kobina, F. The Influence of Geological Factors and Transmission Fluids on the Exploitation of Reservoir Geothermal Resources: Factor Discussion and Mechanism Analysis. *Reserv. Sci.* **2025**, *1*, 3–18. [CrossRef]
33. Li, X.; Li, G.; Wang, H.; Tian, S.; Song, X.; Lu, P.; Wang, M. A unified model for wellbore flow and heat transfer in pure CO_2 injection for geological sequestration, EOR and fracturing operations. *Int. J. Greenhouse Gas Control* **2017**, *57*, 102–115. [CrossRef]
34. Deng, Z.; Fan, Y.; Theuerkauf, J.; Jacob, K.V.; Umbanhowar, P.B.; Lueptow, R.M. Modeling segregation of polydisperse granular materials in hopper discharge. *Powder Technol.* **2020**, *374*, 389–398. [CrossRef]
35. Zhou, Z.; Jin, G.; Liu, Y.; Gao, C.; Ma, H.; Bai, S.; Song, J. A coarse-grained CFD-DEM method for efficient simulation of fluid-solid coupling failure process in geomaterials: Methodology and verification. *Powder Technol.* **2025**, *467*, 121483. [CrossRef]
36. Han, L.; Shi, X.; Ni, H.; Zhang, W.; Gao, Q. Review of CO_2 fracturing and carbon storage in shale reservoirs. *Energy Fuels* **2024**, *38*, 15913–15934. [CrossRef]
37. Middleton, R.; Viswanathan, H.; Currier, R.; Gupta, R. CO_2 as a fracturing fluid: Potential for commercial-scale shale gas production and CO_2 sequestration. *Energy Procedia* **2014**, *63*, 7780–7784. [CrossRef]
38. Wu, J.; Ansari, U. From CO_2 Sequestration to Hydrogen Storage: Further Utilization of Depleted Gas Reservoirs. *Reserv. Sci.* **2025**, *1*, 19–35. [CrossRef]
39. Li, Q.; Wang, Y.; Wang, Y.; San, J.; Li, Q.; Foster, G. Synthetic process on hydroxyl-containing polydimethylsiloxane as a thickener in CO_2 fracturing and thickening performance test. *Energy Sources Part A Recovery Util. Environ. Eff.* **2018**, *40*, 1137–1143. [CrossRef]
40. Wang, K.; Chang, C. Study on the characteristics of CO_2 fracturing rock damage based on fractal theory. *Theor. Appl. Fract. Mech.* **2024**, *134*, 104691. [CrossRef]
41. Zhang, Y.; Niu, Z.; Yang, F.; Ma, Z. Improved equation of state model for the phase behavior of CO_2–hydrocarbon coupling nanopore confinements. *Nat. Gas Ind. B* **2025**, *12*, 316–327. [CrossRef]
42. Middleton, R.S.; Carey, J.W.; Currier, R.P.; Hyman, J.D.; Kang, Q.; Karra, S.; Jiménez-Martínez, J.; Porter, M.L.; Viswanathan, H.S. Shale gas and non-aqueous fracturing fluids: Opportunities and challenges for supercritical CO_2. *Appl. Energy* **2015**, *147*, 500–509. [CrossRef]
43. Ha, S.J.; Choo, J.; Yun, T.S. Liquid CO_2 fracturing: Effect of fluid permeation on the breakdown pressure and cracking behavior. *Rock Mech. Rock Eng.* **2018**, *51*, 3407–3420. [CrossRef]
44. Yang, Y.; Li, Q.; Xu, Y.; Huang, J. Dynamics study of self-pulling self-rotating jet drill bit in natural gas hydrate reservoirs radial horizontal well drilling. *Geoenergy Sci. Eng.* **2025**, *244*, 213490. [CrossRef]
45. Cao, L.; Lv, M.; Li, C.; Sun, Q.; Wu, M.; Xu, C.; Dou, J. Effects of Crosslinking Agents and Reservoir Conditions on the Propagation of Fractures in Coal Reservoirs During Hydraulic Fracturing. *Reserv. Sci.* **2025**, *1*, 36–51. [CrossRef]
46. Guo, T.; Yang, X.; Liu, H.; Chen, M.; Hu, Z.; Niu, J.; Shi, Y. Numerical simulation of proppant transport from a horizontal well into a perforation using computational fluid dynamics. *Nat. Gas Ind. B* **2023**, *10*, 341–351. [CrossRef]
47. Xiao, F.; Salimzadeh, S.; Zhang, Q.B. A 3D coupled numerical simulation of energised fracturing with CO_2: Impact of CO_2 phase on fracturing process. *Int. J. Rock Mech. Min. Sci.* **2024**, *182*, 105863. [CrossRef]
48. Cao, Y.; Zhang, J.; Zhai, H.; Fu, G.; Tian, L.; Liu, S. CO_2 gas fracturing: A novel reservoir stimulation technology in low permeability gassy coal seams. *Fuel* **2017**, *203*, 197–207. [CrossRef]
49. Wang, H.; Li, G.; Zhu, B.; Sepehrnoori, K.; Shi, L.; Zheng, Y.; Shi, X. Key problems and solutions in supercritical CO_2 fracturing technology. *Front. Energy* **2019**, *13*, 667–672. [CrossRef]
50. He, L.; Feng, W.; Siwei, M.; Yongwei, D. Fracturing with carbon dioxide: Application status and development trend. *Pet. Explor. Dev.* **2014**, *41*, 513–519. [CrossRef]
51. Li, M.; Liu, J.; Xia, Y. Risk Prediction of Gas Hydrate Formation in the Wellbore and Subsea Gathering System of Deep-Water Turbidite Reservoirs: Case Analysis from the South China Sea. *Reserv. Sci.* **2025**, *1*, 52–72. [CrossRef]
52. Jiang, Z.; Quan, X.; Tian, S.; Liu, H.; Guo, Y.; Fu, X.; Yang, X. Permeability-enhancing technology through liquid CO_2 fracturing and its application. *Sustainability* **2022**, *14*, 10438. [CrossRef]
53. Pruess, K. Enhanced geothermal systems (EGS) using CO_2 as working fluid—A novel approach for generating renewable energy with simultaneous sequestration of carbon. *Geothermics* **2006**, *35*, 351–367. [CrossRef]
54. Li, Q.; Li, Q.; Cao, H.; Wu, J.; Wang, F.; Wang, Y. The Crack Propagation Behaviour of CO_2 Fracturing Fluid in Unconventional Low Permeability Reservoirs: Factor Analysis and Mechanism Revelation. *Processes* **2025**, *13*, 159. [CrossRef]
55. Li, Q.; Wang, F.; Wang, Y.; Bai, B.; Zhang, J.; Lili, C.; Forson, K. Adsorption behavior and mechanism analysis of siloxane thickener for CO_2 fracturing fluid on shallow shale soil. *J. Mol. Liq.* **2023**, *376*, 121394. [CrossRef]
56. Liu, L.; Zhu, W.; Wei, C.; Elsworth, D.; Wang, J. Microcrack-based geomechanical modeling of rock-gas interaction during supercritical CO_2 fracturing. *J. Pet. Sci. Eng.* **2018**, *164*, 91–102. [CrossRef]

57. Shi, W.; Zhu, L.; Guo, M.; Huang, Z.; Wang, G.; Lin, L.; He, L.; Liao, Y.; He, H.; Gong, J. Assessment of CO_2 fracturing in China's shale oil reservoir: Fracturing effectiveness and carbon storage potential. *Resour. Conserv. Recycl.* **2023**, *197*, 107101. [CrossRef]
58. Zhang, F.Z.; Jiang, P.X.; Xu, R.N. System thermodynamic performance comparison of CO_2-EGS and water-EGS systems. *Appl. Therm. Eng.* **2013**, *61*, 236–244. [CrossRef]
59. Li, Q.; Li, Q.; Wu, J.; Li, X.; Li, H.; Cheng, Y. Wellhead stability during development process of hydrate reservoir in the Northern South China Sea: Evolution and mechanism. *Processes* **2025**, *13*, 40. [CrossRef]
60. Wang, Z.; Sun, B.; Sun, X. Calculation of temperature in fracture for carbon dioxide fracturing. *SPE J.* **2016**, *21*, 1491–1500. [CrossRef]
61. Wang, J.; Wang, Z.; Sun, B.; Gao, Y.; Wang, X.; Fu, W. Optimization design of hydraulic parameters for supercritical CO_2 fracturing in unconventional gas reservoir. *Fuel* **2019**, *235*, 795–809. [CrossRef]
62. Zhang, W.; Wang, C.; Guo, T.; He, J.; Zhang, L.; Chen, S.; Qu, Z. Study on the cracking mechanism of hydraulic and supercritical CO_2 fracturing in hot dry rock under thermal stress. *Energy* **2021**, *221*, 119886. [CrossRef]
63. Song, X.; Guo, Y.; Zhang, J.; Sun, N.; Shen, G.; Chang, X.; Yu, W.; Tang, Z.; Chen, W.; Wei, W.; et al. Fracturing with carbon dioxide: From microscopic mechanism to reservoir application. *Joule* **2019**, *3*, 1913–1926. [CrossRef]
64. Li, Y.; Peng, G.; Tang, J.; Zhang, J.; Zhao, W.; Liu, B.; Pan, Y. Thermo-hydro-mechanical coupling simulation for fracture propagation in CO_2 fracturing based on phase-field model. *Energy* **2023**, *284*, 128629. [CrossRef]
65. Ma, D.; Wu, Y.; Ma, X.; Hu, D.; Zhou, H.; Li, D. A preliminary experimental and numerical study on the applicability of liquid CO_2 fracturing in sparse sandstone. *Rock Mech. Rock Eng.* **2023**, *56*, 7315–7332. [CrossRef]
66. Ao, F.; Qingchao, L.; Qiang, L.; Jingjuan, W.; Fuling, W.; Chuanliang, Y. Numerical Simulation Investigation of Fracture Propagation Behavior Patterns and Sensitivity Factors of Oil Shale Reservoirs in the Xunyi Region Considering the Influence of Natural Fracture. *Geofluids* **2025**, *2025*, 2762142. [CrossRef]
67. Qin, F.; Cai, Z.; Ming, H.; Zhang, F.; He, Z.; Zhu, C.; Li, D. Calculation Models for Vapor-liquid Phase Equilibrium in Mixture Systems of CO_2 Containing Impurities. *Pet. New Energy* **2024**, *36*, 87–96.
68. Takuma, K.; Maeda, Y.; Watanabe, Y.; Ogata, S.; Sakaguchi, K.; Pramudyo, E.; Fukuda, D.; Wang, J.; Osato, K.; Terai, A.; et al. CO_2 fracturing of volcanic rocks under geothermal conditions: Characteristics and process. *Geothermics* **2024**, *120*, 103007. [CrossRef]
69. Wang, K.; Pan, H.; Fujii, Y. Study on energy distribution and attenuation of CO_2 fracturing vibration from coal-like material in a new test platform. *Fuel* **2024**, *356*, 129584. [CrossRef]
70. Mollaali, M.; Ziaei-Rad, V.; Shen, Y. Numerical modeling of CO_2 fracturing by the phase field approach. *J. Nat. Gas Sci. Eng.* **2019**, *70*, 102905. [CrossRef]
71. Li, Q.; Wang, F.; Wang, Y.; Zhou, C.; Chen, J.; Forson, K.; Zhang, J. Effect of reservoir characteristics and chemicals on filtration property of water-based drilling fluid in unconventional reservoir and mechanism disclosure. *Environ. Sci. Pollut. Res.* **2023**, *30*, 55034–55043. [CrossRef]
72. Qiao, Y.; Wang, N.; Li, Y.; Luo, W.; Teng, B. Study on the Influence Mechanism of Natural Fracture Characteristics on EUR of Gas Wells in Horizontal Well Development of Deep Shale Gas. *Pet. New Energy* **2025**, *37*, 71–78.
73. He, W.; Lian, H.; Liang, W.; Wu, P.; Jiang, Y.; Song, X. Experimental study of supercritical CO_2 fracturing across coal–rock interfaces. *Rock Mech. Rock Eng.* **2023**, *56*, 57–68. [CrossRef]
74. Belousov, A.; Lushpeev, V.; Sokolov, A.; Sultanbekov, R.; Tyan, Y.; Ovchinnikov, E.; Islamov, S. Hartmann–sprenger energy separation effect for the quasi-isothermal pressure reduction of natural gas: Feasibility analysis and numerical simulation. *Energies* **2024**, *17*, 2010. [CrossRef]
75. Li, Q.; Li, Q.; Wang, F.; Xu, N.; Wang, Y.; Bai, B. Settling behavior and mechanism analysis of kaolinite as a fracture proppant of hydrocarbon reservoirs in CO_2 fracturing fluid. *Colloids Surf. A Physicochem. Eng. Asp.* **2025**, *724*, 137463. [CrossRef]
76. Li, S.; Zhang, S.; Ma, X.; Zou, Y.; Li, N.; Wu, S.; Zhang, Z. Coupled physical–chemical effects of CO_2 on rock properties and breakdown during intermittent CO_2-hybrid fracturing. *Rock Mech. Rock Eng.* **2020**, *53*, 1665–1683. [CrossRef]
77. Ma, D.; Cheng, C.; Ding, C.; Song, J.; Hu, D.; Zhou, H. Comparisons of fracturing mechanism of tight sandstone using liquid CO_2 and water. *J. Nat. Gas Sci. Eng.* **2021**, *94*, 104108. [CrossRef]
78. Meng, S.; Zhang, F.; Tao, J.; Jin, X.; Xu, J.; Liu, H. Carbon storage potential of shale reservoirs based on CO_2 fracturing technology. *Engineering* **2025**, *48*, 121–127. [CrossRef]
79. Li, Q.; Cheng, Y.; Li, Q.; Zhang, C.; Ansari, U.; Song, B. Establishment and evaluation of strength criterion for clayey silt hydrate-bearing sediments. *Energy Sources Part A Recovery Util. Environ. Eff.* **2018**, *40*, 742–750. [CrossRef]
80. Zhang, L.; Cao, C.; Wen, S.; Zhao, Y.; Peng, X.; Wu, J. Thoughts on the development of CO_2-EGR under the background of carbon peak and carbon neutrality. *Nat. Gas Ind. B* **2023**, *10*, 383–392. [CrossRef]
81. Wang, J.; Sun, B.; Li, H.; Wang, X.; Wang, Z.; Sun, X. Phase state control model of supercritical CO_2 fracturing by temperature control. *Int. J. Heat Mass Transf.* **2018**, *118*, 1012–1021. [CrossRef]
82. Hölzer, A.; Sommerfeld, M. New simple correlation formula for the drag coefficient of non-spherical particles. *Powder Technol.* **2008**, *184*, 361–365. [CrossRef]

83. Haider, A.; Levenspiel, O. Drag coefficient and terminal velocity of spherical and nonspherical particles. *Powder Technol.* **1989**, *58*, 63–70. [CrossRef]
84. Yan, H.; Zhang, J.; Zhou, N.; Li, M. Staged numerical simulations of supercritical CO_2 fracturing of coal seams based on the extended finite element method. *J. Nat. Gas Sci. Eng.* **2019**, *65*, 275–283. [CrossRef]
85. Memon, S.; Feng, R.; Ali, M.; Bhatti, M.A.; Giwelli, A.; Keshavarz, A.; Xie, Q.; Sarmadivaleh, M. Supercritical CO_2-Shale interaction induced natural fracture closure: Implications for $scCO_2$ hydraulic fracturing in shales. *Fuel* **2022**, *313*, 122682. [CrossRef]
86. Garbis, S.J.; Taylor, J.L. The utility of CO_2 as an energizing component for fracturing fluids. *SPE Prod. Eng.* **1986**, *1*, 351–358. [CrossRef]
87. Cao, Y.; Liu, T.; Song, G.; Hu, Y.; Li, Y.; Zhou, W.; Han, H.; Li, Y. Experimental Study on Temperature Drop Characteristics of Supercritical CO_2 Leakage on Offshore Platform. *Pet. New Energy* **2024**, *36*, 20–25.
88. Li, Q.; Cheng, Y.; Li, Q.; Ansari, U.; Liu, Y.; Yan, C.; Lei, C. Development and verification of the comprehensive model for physical properties of hydrate sediment. *Arab. J. Geosci.* **2018**, *11*, 1–16. [CrossRef]
89. Zhang, G.; Wu, T.; Li, J.; Pang, Q.; Yang, H.; Liu, G.; Huang, H.; Zhu, Y. Dynamics simulation of the effect of cosolvent on the solubility and tackifying behavior of PDMS tackifier in supercritical CO_2 fracturing fluid. *Colloids Surf. A: Physicochem. Eng. Asp.* **2023**, *662*, 130985. [CrossRef]
90. Yang, Y.; Huang, F.; Xu, Y.; He, J.; Deng, D.; Zhan, S.; Zhang, C. Dynamics study of hot dry rock percussive drilling tool based on the drill string axial vibration. *Geoenergy Sci. Eng.* **2025**, *246*, 213599. [CrossRef]
91. Li, C.; Huang, Y.; Sun, X.; Gao, R.; Zeng, F.B.; Tontiwachwuthikul, P.; Liang, Z. Rheological properties study of foam fracturing fluid using CO_2 and surfactant. *Chem. Eng. Sci.* **2017**, *170*, 720–730. [CrossRef]
92. Yang, Z.; Luo, W.; Zhang, L.; Zhu, J.; Li, X.; Zhao, Y.; Chen, X.; Liu, C. A molecular dynamics investigation into the polymer tackifiers in supercritical CO_2 fracturing fluids under wellbore conditions. *J. Supercrit. Fluids* **2024**, *212*, 106352. [CrossRef]
93. Jiang, C.; Jing, C.; Wang, H.; Wang, L.; Zhang, L. Phase-field simulation of CO_2 fracturing crack propagation in thermo-poroelastic media. *Int. J. Rock Mech. Min. Sci.* **2025**, *187*, 106052. [CrossRef]
94. Liu, H.; Liu, G.; Zhang, Z.; Li, B.; Si, N.; Guan, W.; Lin, J. Effects of liquid CO_2 phase transition fracturing on mesopores and micropores in coal. *Energy Fuels* **2022**, *36*, 10016–10025. [CrossRef]
95. Al-Hajri, S.; Negash, B.M.; Rahman, M.M.; Haroun, M.; Al-Shami, T.M. Perspective Review of polymers as additives in water-based fracturing fluids. *ACS Omega* **2022**, *7*, 7431–7443. [CrossRef] [PubMed]
96. Xue, S.; Huang, Q.; Wang, G.; Bing, W.; Li, J. Experimental study of the influence of water-based fracturing fluids on the pore structure of coal. *J. Nat. Gas Sci. Eng.* **2021**, *88*, 103863. [CrossRef]
97. Fan, J.; Morris, G.L. Reservoir sedimentation. II: Reservoir desiltation and long-term storage capacity. *J. Hydraul. Eng.* **1992**, *118*, 370–384. [CrossRef]
98. Dutta, S. Soil erosion, sediment yield and sedimentation of reservoir: A review. *Model. Earth Syst. Environ.* **2016**, *2*, 123. [CrossRef]
99. Baiyu, Z.; Hongming, T.; Senlin, Y.; Gongyang, C.; Feng, Z.; Shiyu, X. Effect of fracture roughness on transport of suspended particles in fracture during drilling. *J. Pet. Sci. Eng.* **2021**, *207*, 109080. [CrossRef]
100. Jain, A.K.; Juanes, R. Preferential mode of gas invasion in sediments: Grain-scale mechanistic model of coupled multiphase fluid flow and sediment mechanics. *J. Geophys. Res. Solid Earth* **2009**, *114*, B08101. [CrossRef]
101. Bjørlykke, K. Relationships between depositional environments, burial history and rock properties. Some principal aspects of diagenetic process in sedimentary basins. *Sediment. Geol.* **2014**, *301*, 1–14. [CrossRef]
102. Cosgrove, J.W. Hydraulic fracturing during the formation and deformation of a basin: A factor in the dewatering of low-permeability sediments. *AAPG Bull.* **2001**, *85*, 737–748. [CrossRef]
103. Tian, F.; Luo, X.; Zhang, W. Integrated geological-geophysical characterizations of deeply buried fractured-vuggy carbonate reservoirs in Ordovician strata, Tarim Basin. *Mar. Pet. Geol.* **2019**, *99*, 292–309. [CrossRef]
104. Liang, Y.; Sui, W.; Qi, J. Experimental investigation on chemical grouting of inclined fracture to control sand and water flow. *Tunn. Undergr. Space Technol.* **2019**, *83*, 82–90. [CrossRef]
105. Chen, X.; Qiu, R.; Wu, X. Multi-timescale capacity configuration optimization of energy storage equipment in power plant-carbon capture system. *Appl. Therm. Eng.* **2023**, *227*, 120371. [CrossRef]
106. Cha, M.; Yin, X.; Kneafsey, T.; Johanson, B.; Alqahtani, N.; Miskimins, J.; Patterson, T.; Wu, Y.S. Cryogenic fracturing for reservoir stimulation–Laboratory studies. *J. Pet. Sci. Eng.* **2014**, *124*, 436–450. [CrossRef]
107. Xiong, C.; Yang, S.H.I.; Fujian, Z.H.O.U.; Xiongfei, L.I.U.; Xianyou, Y.A.N.G.; Xiangtong, Y.A.N.G. High efficiency reservoir stimulation based on temporary plugging and diverting for deep reservoirs. *Pet. Explor. Dev.* **2018**, *45*, 948–954. [CrossRef]
108. Panahov, G.M.; Abbasov, E.M.; Jiang, R. The novel technology for reservoir stimulation: In situ generation of carbon dioxide for the residual oil recovery. *J. Pet. Explor. Prod.* **2021**, *11*, 2009–2026. [CrossRef]
109. Guo, J.; Gou, B.; Qin, N.; Zhao, J.; Wu, L.; Wang, K.; Ren, J. An innovative concept on deep carbonate reservoir stimulation: Three-dimensional acid fracturing technology. *Nat. Gas Ind. B* **2020**, *7*, 484–497. [CrossRef]

110. Li, N.; Xie, H.; Hu, J.; Li, C. A critical review of the experimental and theoretical research on cyclic hydraulic fracturing for geothermal reservoir stimulation. *Geomech. Geophys. Geo-Energy Geo-Resour.* **2022**, *8*, 7. [CrossRef]
111. Jianchun, G.; Cong, L.; Yong, X.; Jichuan, R.; Chaoyi, S.; Yu, S. Reservoir stimulation techniques to minimize skin factor of Longwangmiao Fm gas reservoirs in the Sichuan Basin. *Nat. Gas Ind. B* **2014**, *1*, 83–88. [CrossRef]
112. Zhang, L.; Pan, L.; Zou, Y.; Wang, J.; Li, M.; Feng, W. Recent advances in reservoir stimulation and enhanced oil recovery technology in unconventional reservoirs. *Processes* **2024**, *12*, 234. [CrossRef]
113. Li, B.; Ma, X.; Zhang, G.; Guo, W.; Xu, T.; Yuan, Y.; Sun, Y. Enhancement of gas production from natural gas hydrate reservoir by reservoir stimulation with the stratification split grouting foam mortar method. *J. Nat. Gas Sci. Eng.* **2020**, *81*, 103473. [CrossRef]
114. Luo, Z.; Zhang, N.; Zhao, L.; Yuan, X.; Zhang, Y. A novel stimulation strategy for developing tight fractured gas reservoir. *Petroleum* **2018**, *4*, 215–222. [CrossRef]
115. Huang, Q.; Liu, S.; Wang, G.; Wu, B.; Zhang, Y. Coalbed methane reservoir stimulation using guar-based fracturing fluid: A review. *J. Nat. Gas Sci. Eng.* **2019**, *66*, 107–125. [CrossRef]

Disclaimer/Publisher's Note: The statements, opinions and data contained in all publications are solely those of the individual author(s) and contributor(s) and not of MDPI and/or the editor(s). MDPI and/or the editor(s) disclaim responsibility for any injury to people or property resulting from any ideas, methods, instructions or products referred to in the content.